Available online at www.sciencedirect.com
ScienceDirect
International Journal of Heat and Mass Transfer 51 (2008) 497–505
International Journal of HEAT and MASS TRANSFER
www.elsevier.com/locate/ijhmt

Low-density lipoprotein (LDL) transport in an artery – A simplified analytical solution

Ning Yang [a], Kambiz Vafai [b,*]

[a] Department of Bioengineering, The Pennsylvania State University, University Park, PA 16803, United States
[b] Department of Mechanical Engineering, University of California, Riverside, CA 92521, United States

Received 11 March 2007; received in revised form 17 May 2007
Available online 15 August 2007

Abstract

An analytical solution is presented for a robust four-layer porous model for the description of the LDL transport in the arterial wall coupled with the transport in the lumen. The endothelium, intima, internal elastic lamina (IEL) and media are all treated as homogenous porous media and modeled using volume-averaged porous media transport equations. The analytical solution is derived based on consideration of primary transport in the lateral direction. The analytical results are found consistent with the numerical data for different physiological conditions. It is clear that the analytical solution offers a good estimation of the LDL transport in a straight geometry.

1. Introduction

Modeling of the macromolecular transport across the arterial wall has received considerable attention in recent years. Several macromolecular transport models have been proposed in the literature. The simplest way is to model the arterial wall by a set of simplified lumen-wall boundary conditions [1–4]. This model, however, can not give any prediction of macromolecular distribution across the wall. A better approach is to model the arterial wall as a homogeneous porous monolayer [5,6]. This model couples the transport of macromolecules in the lumen with their transport across the arterial wall. A set of more realistic boundary condition are applied at the wall-lumen interface by mass balance. The most comprehensive models are multi-layer models [7–15]. In these models, the arterial wall is modeled as several different porous layers, i.e. endothelium, intima, IEL, and media. The Staverman–Kedem–Katchalsky membrane equations are used to model the macromolecular transport in the endothelium and IEL layers.

Yang and Vafai [15] developed a robust multi-layer porous model for the description of the mass transport in the arterial wall coupled with the mass transport in the arterial lumen. In this model, the endothelium, intima, IEL and media layers of the artery are all treated as macroscopically homogenous porous media and mathematically modeled using proper types of the volume averaged porous media equations, with the Staverman filtration and osmotic reflection coefficients employed to account for selective permeability of each porous layer to certain solutes. In their study, it is found that the LDL transport in the arterial wall is one-dimensional when a straight circular geometry is considered.

The main purpose of the present study is to derive an analytical solution for the porous multi-layer model developed by Yang and Vafai based on the primary preferred lateral transport. The analytical solution is found to be consistent with the more comprehensive numerical results for different physiological conditions. The good agreement between the numerical and analytical solutions will lead the way for a highly efficient methodology to quantitatively

* Corresponding author. Tel.: +1 951 827 2135; fax: +1 951 827 2899.
E-mail address: vafai@engr.ucr.edu (K. Vafai).

0017-9310/$ - see front matter © 2007 Elsevier Ltd. All rights reserved.
doi:10.1016/j.ijheatmasstransfer.2007.05.023

Nomenclature

C	dimensionless LDL concentration, $\frac{c}{C_0}$
$C^+_{\text{adventitia}}$	dimensionless LDL concentration at the media–adventitia interface
C^+_{lumen}	dimensionless LDL concentration at the lumen endothelium interface
C_0	reference inflow LDL concentration [nmol/mm^3]
c	dimensional LDL concentration [nmol/mm^3]
$\overline{c}$	average LDL concentration
D	diffusivity [mm^2/s]
Da	Darcy number, $\frac{K}{L_0^2}$
K	permeability [mm^2]
k	effective volumetric first-order reaction rate coefficient [1/s]
L	longitudinal length of the artery [mm]
L_0	reference length [mm]
n	normal direction
Pe	Peclet number, $\frac{U_0 L_0}{D_e}$
p	hydraulic pressure
R	radius of the arterial lumen [mm]
Re	Reynolds number, $\frac{\rho U_0 L_0}{\mu}$
R_u	universal gas constant
r	dimensional radial coordinate [mm]
T	absolute temperature [K]
t	dimensional time [s]
U_0	reference bulk inflow velocity [mm/s]
u	dimensional axial velocity [mm/s]
V	velocity vector [mm/s]
V_0	reference filtration velocity [mm/s]
v	dimensional radial velocity [mm/s]
x	dimensional axial coordinate [mm]

Greek symbols

ε	porosity
μ	dynamic viscosity [g/(mm s)]
μ'	effective dynamic viscosity of a medium [g/(mm s)]
π	osmotic pressure
ρ	density [g/mm^3]
σ_d	Staverman osmotic reflection coefficient
σ_f	Staverman filtration reflection coefficient

Superscripts

f	fluid
*	dimensionless parameter

Subscripts

adventitia	adventitia
e	effective property
endo	endothelium
IEL	internal elastic lamina
int	intima
med	media

Other symbol

$\langle\rangle$	'local volume average' of a quantity

analyze how the LDL transport through the arterial wall is related to the atherosclerosis.

2. Mathematical formulation

The arterial wall layers, i.e. endothelium, intima, IEL, and media, are treated as macroscopically homogenous porous media. The details of the model description are presented in [15]. The governing equations for each layer are described as follows:

2.1. Lumen

The blood is modeled as an incompressible Newtonian flow:

$$\rho\frac{\partial V}{\partial t}+\rho V\cdot\nabla V=-\nabla p+\mu\nabla^2 V \tag{1}$$

$$\nabla\cdot V=0 \tag{2}$$

where V is the velocity vector, p the pressure, and ρ and μ are the density and dynamic viscosity of blood.

The mass transport equation in the lumen is:

$$\frac{\partial c}{\partial t}+V\cdot\nabla c=D\nabla^2 c \tag{3}$$

where c is the LDL concentration and D is the LDL diffusivity within the blood.

2.1.1. Endothelium and internal elastic lamina

The endothelium and internal elastic lamina (IEL) are considered as macroscopically homogenous porous media and modeled as follows:

$$\nabla\cdot\langle V\rangle=0 \tag{4}$$

$$\frac{\rho}{\varepsilon}\frac{\partial\langle V\rangle}{\partial t}+\frac{\mu}{K}\langle V\rangle=-\nabla\langle p\rangle^f+R_u T\sigma_d\nabla\langle c\rangle+\mu'\nabla^2\langle V\rangle \tag{5}$$

$$\frac{\partial\langle c\rangle}{\partial t}+(1-\sigma_f)\langle V\rangle\cdot\nabla\langle c\rangle=D_e\nabla^2\langle c\rangle \tag{6}$$

where ε is the porosity, K the hydraulic permeability, μ' the effective dynamic viscosity of the medium and D_e is the effective LDL diffusivity in the medium. The parameters σ_f and σ_d are the Staverman filtration and osmotic reflection coefficients, respectively, T the absolute temperature of the medium, and R_u is the universal gas constant. The symbol "$\langle\rangle$" denotes the local volume average of a quantity

and the superscript f refers to the local volume average inside the fluid.

2.1.2. Intima and media

The governing equations for intima and media are presented as follows:

$$\nabla \cdot \langle V \rangle = 0 \tag{7}$$

$$\frac{\rho}{\varepsilon}\frac{\partial \langle V \rangle}{\partial t} + \frac{\mu}{K}\langle V \rangle = -\nabla \langle p \rangle^f + \mu' \nabla^2 \langle V \rangle \tag{8}$$

$$\frac{\partial \langle c \rangle}{\partial t} + (1-\sigma_f)\langle V \rangle \cdot \nabla \langle c \rangle = D_e \nabla^2 \langle c \rangle + k\langle c \rangle \tag{9}$$

where k is the effective volumetric first-order reaction rate coefficient. For these layers, the osmotic effect in the transport is neglected when compared to the hydraulic pressure. Note that from here on the symbol "$\langle\rangle$" indicating averaged values will be dropped for simplicity.

3. Analytical solutions

Eqs. (1)–(9) can be solved analytically if a straight pipe geometry (Fig. 1) is considered. As cited by Yang and Vafai [15], for a straight circular geometry, the filtration velocity in the axial direction is much smaller than the filtration velocity in the radial direction. As a result, the LDL transport within the arterial wall can be assumed to be independent of the axial direction. The osmotic effect in the endothelium and IEL is negligible [15]. To further simplify the problem, the effects of solid boundaries are not included in the momentum equations for different porous layers. It is also shown in [15] that pulsatile flows have a negligible impact on the LDL transport within the arterial wall for a straight circular geometry. This appears to be mainly due to the damping effects of the arterial wall. Therefore the transient effects are neglected in this work. The hydraulic pressure at the lumen endothelium interface is taken as 100 mmHg, which is fairly reasonable for the present study [15]. With a proper species boundary condition applied at the lumen endothelium interface, Eqs. (4)–(9) are solved to obtain an analytical solution for the LDL species distribution across the arterial wall.

Based on these assumptions, Eqs. (4)–(9) can be simplified as:

Endothelium and Intima and IEL:

$$\frac{1}{Re\,Da}v^* = -\frac{\partial p^*}{\partial y^*} \tag{10}$$

$$(1-\sigma^f)v^*\frac{\partial C}{\partial y^*} = \frac{1}{Pe}\frac{\partial^2 C}{\partial y^{*2}} \tag{11}$$

$$\frac{\partial v^*}{\partial y^*} = 0 \tag{12}$$

Media:

$$\frac{1}{Re\,Da}v^* = -\frac{\partial p^*}{\partial y^*} \tag{13}$$

$$(1-\sigma^f)v^*\frac{\partial C}{\partial y^*} = \frac{1}{Pe}\frac{\partial^2 C}{\partial y^{*2}} + \frac{kL_0}{V_0}C \tag{14}$$

$$\frac{\partial v^*}{\partial y^*} = 0 \tag{15}$$

where the dimensionless parameters are defined as follows:

$$v^* = \frac{v}{V_0};\quad C = \frac{c}{C_0};\quad p^* = \frac{p}{\rho V_0^2};\quad y^* = \frac{y}{L_0};$$
$$Re = \frac{\rho V_0 L_0}{\mu};\quad Da = \frac{K}{L_0^2};\quad Pe = \frac{V_0 L_0}{D_e} \tag{16}$$

where v is the filtration velocity in the radial direction and y is the coordinate along the radial direction. In the present study the reference filtration velocity V_0 is chosen as 2.31×10^{-5} mm/s, which is consistent with the numerical data in [15], and the reference length L_0 is chosen as the thickness of the arterial wall, which is equal to 214 μm [15]. It should be noted that the effect of curvature is

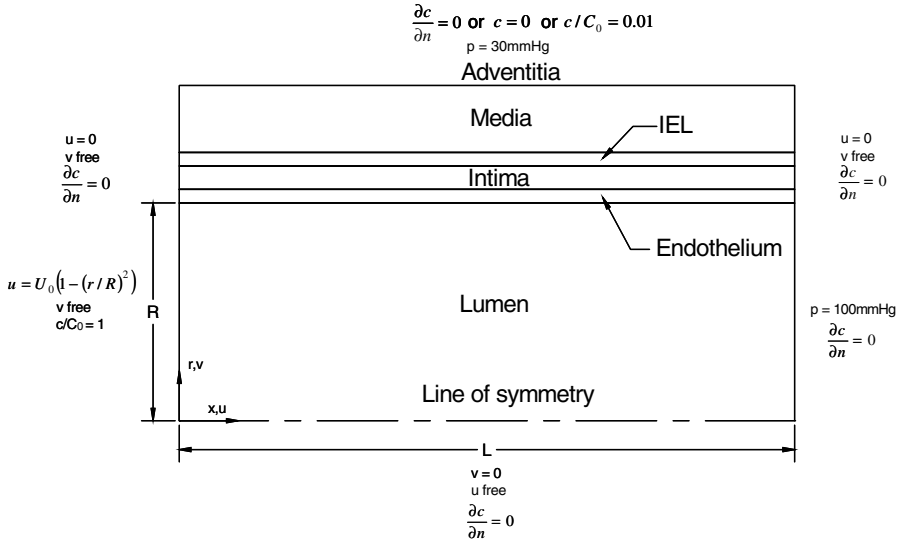

Fig. 1. Schematic illustration of the geometric artery.

negligible since the thickness of the arterial wall is small when compared to the overall radius of the artery.

The boundary conditions for the momentum equations at the lumen–endothelium and media–adventitia interfaces are:

$$p^*(y^*=0)=p_1^*;\quad p^*(y^*=1)=p_2^* \tag{17}$$

where p_1^* and p_2^* are defined as

$$p_1^*=\frac{p_1}{\rho V_0^2};\quad p_2^*=\frac{p_2}{\rho V_0^2} \tag{18}$$

where p_2 is chosen as 30 mmHg [15]. At the interfaces between the lumen, endothelium, intima, IEL and media continuity of velocity is applied.

The dimensionless concentration boundary condition at the lumen endothelium interface is assumed to be

$$C(y^*=0)=C^+_{\text{lumen}} \tag{19}$$

The corresponding concentration boundary conditions at the interface between the endothelium, intima, IEL and media are the continuity of the species concentration and total mass flux, which can be represented as

$$\left[(1-\sigma_f)v^*C-\frac{1}{Pe}\frac{\partial C}{\partial y^*}\right]\Big|_+=\left[(1-\sigma_f)v^*C-\frac{1}{Pe}\frac{\partial C}{\partial y^*}\right]\Big|_- \tag{20}$$

The concentration boundary conditions at the media–adventitia interface are

$$\frac{\partial C}{\partial y^*}=0\quad\text{and}\quad C(y^*=1)=C^+_{\text{adventitia}} \tag{21}$$

Eqs. (10)–(16) are solved analytically subject to boundary conditions (17)–(21) applied. The hydraulic resistance for each layer can be written as

$$R=\frac{L^*}{ReDa} \tag{22}$$

The filtration velocity through the arterial wall can be predicted in terms of the hydraulic driving force, pressure difference, and the total hydraulic resistance, as

$$v^*=\frac{p_1^*-p_2^*}{\left(\frac{L^*}{ReDa}\right)_{\text{endo}}+\left(\frac{L^*}{ReDa}\right)_{\text{intima}}+\left(\frac{L^*}{ReDa}\right)_{\text{IEL}}+\left(\frac{L^*}{ReDa}\right)_{\text{media}}} \tag{23}$$

where L^* is the dimensionless thickness of each of the porous layers.

The mass transport equations of the endothelium, intima, IEL and media can be readily obtained as

$$C(y^*)=c_1e^{\lambda_1 y^*}+c_2e^{\lambda_2 y^*} \tag{24}$$

where c_1 and c_2 are constant. For the endothelium, intima and IEL, λ_1 and λ_2 can be expressed as

$$\lambda_1=Pe(1-\sigma^f)v^*;\quad \lambda_2=0 \tag{25}$$

For the media, λ_1 and λ_2 are given as

$$(\lambda_{1,2})_{\text{media}}=\frac{Pe(1-\sigma^f)v^*\pm\sqrt{(Pe(1-\sigma^f)v^*)^2-\frac{4kL_0Pe}{V_0}}}{2} \tag{26}$$

Applying boundary conditions (19)–(21) to Eq. (24) results:

$$c_1^{\text{endo}}+c_2^{\text{endo}}=C^+_{\text{lumen}} \tag{27}$$

$$c_1^{\text{endo}}e^{\lambda_1^{\text{endo}}L^*_{\text{endo}}}+c_2^{\text{endo}}=c_1^{\text{int}}e^{\lambda_1^{\text{int}}L^*_{\text{endo}}}+c_2^{\text{int}} \tag{28}$$

$$\begin{aligned}&v^*(1-\sigma_f^{\text{end}})(c_1^{\text{end}}e^{\lambda_1^{\text{end}}L^*_{\text{end}}}+c_2^{\text{end}})-\frac{1}{Pe^{\text{end}}}c_1^{\text{end}}\lambda_1^{\text{end}}e^{\lambda_1^{\text{end}}L^*_{\text{end}}}\\&=v^*(1-\sigma_f^{\text{int}})(c_1^{\text{int}}e^{\lambda_1^{\text{int}}L^*_{\text{end}}}+c_2^{\text{int}})\\&-\frac{1}{Pe^{\text{int}}}c_1^{\text{int}}\lambda_1^{\text{int}}e^{\lambda_1^{\text{int}}L^*_{\text{end}}}\end{aligned} \tag{29}$$

$$c_1^{\text{int}}e^{\lambda_1^{\text{int}}(L^*_{\text{end}}+L^*_{\text{int}})}+c_2^{\text{int}}=c_1^{\text{IEL}}e^{\lambda_1^{\text{IEL}}(L^*_{\text{end}}+L^*_{\text{int}})}+c_2^{\text{IEL}} \tag{30}$$

$$\begin{aligned}&v^*(1-\sigma_f^{\text{int}})(c_1^{\text{int}}e^{\lambda_1^{\text{int}}(L^*_{\text{end}}+L^*_{\text{int}})}+c_2^{\text{int}})-\frac{1}{Pe^{\text{int}}}c_1^{\text{int}}\lambda_1^{\text{int}}e^{\lambda_1^{\text{int}}(L^*_{\text{end}}+L^*_{\text{int}})}\\&=v^*(1-\sigma_f^{\text{IEL}})(c_1^{\text{IEL}}e^{\lambda_1^{\text{IEL}}(L^*_{\text{end}}+L^*_{\text{int}})}+c_2^{\text{IEL}})\\&-\frac{1}{Pe^{\text{IEL}}}c_1^{\text{IEL}}\lambda_1^{\text{IEL}}e^{\lambda_1^{\text{IEL}}(L^*_{\text{endt}}+L^*_{\text{int}})}\end{aligned} \tag{31}$$

$$\begin{aligned}&c_1^{\text{IEL}}e^{\lambda_1^{\text{IEL}}(L^*_{\text{end}}+L^*_{\text{int}}+L^*_{\text{IEL}})}+c_2^{\text{IEL}}\\&=c_1^{\text{med}}e^{\lambda_1^{\text{med}}(L^*_{\text{end}}+L^*_{\text{int}}+L^*_{\text{IEL}})}+c_2^{\text{med}}e^{\lambda_2^{\text{med}}(L^*_{\text{end}}+L^*_{\text{int}}+L^*_{\text{IEL}})}\end{aligned} \tag{32}$$

$$\begin{aligned}&v^*(1-\sigma_f^{\text{IEL}})(c_1^{\text{IEL}}e^{\lambda_1^{\text{IEL}}(L^*_{\text{end}}+L^*_{\text{int}}+L^*_{\text{IEL}})}+c_2^{\text{IEL}})\\&-\frac{1}{Pe^{\text{IEL}}}c_1^{\text{IEL}}\lambda_1^{\text{IEL}}e^{\lambda_1^{\text{IEL}}(L^*_{\text{endt}}+L^*_{\text{int}}+L^*_{\text{IEL}})}=v^*(1-\sigma_f^{\text{med}})(c_1^{\text{med}}e^{\lambda_1^{\text{med}}(L^*_{\text{endt}}+L^*_{\text{int}}+L^*_{\text{IEL}})}\\&+c_2^{\text{med}}e^{\lambda_2^{\text{med}}(L^*_{\text{endt}}+L^*_{\text{int}}+L^*_{\text{IEL}})})-\frac{1}{Pe^{\text{med}}}(c_1^{\text{med}}\lambda_1^{\text{med}}e^{\lambda_1^{\text{med}}(L^*_{\text{end}}+L^*_{\text{int}}+L^*_{\text{IEL}})}\\&+c_2^{\text{med}}\lambda_2^{\text{med}}e^{\lambda_2^{\text{med}}(L^*_{\text{end}}+L^*_{\text{int}}+L^*_{\text{IEL}})})\end{aligned} \tag{33}$$

$$c_1^{\text{med}}\lambda_1^{\text{med}}e^{\lambda_1^{\text{med}}(L^*_{\text{end}}+L^*_{\text{int}}+L^*_{\text{IEL}}+L^*_{\text{med}})}+c_2^{\text{med}}\lambda_2^{\text{med}}e^{\lambda_2^{\text{med}}(L^*_{\text{end}}+L^*_{\text{int}}+L^*_{\text{IEL}}+L^*_{\text{med}})}=0 \tag{34}$$

where subscripts "lumen", "endo", "int", "IEL" and "med" refer to the lumen, endothelium, intima, IEL, and media respectively. Eq. (34) is derived based on the boundary condition, $\frac{\partial C}{\partial y^*}=0$, applied at the media-adventitia interface.

Eqs. (27)–(34) can be rearranged in a matrix form as

$$AC=B \tag{35}$$

where matrix A and vectors B and C are:

$$A=\begin{bmatrix}A_{11}&A_{12}&0&0&0&0&0&0\\A_{21}&A_{22}&A_{23}&A_{24}&0&0&0&0\\A_{31}&A_{32}&A_{33}&A_{34}&0&0&0&0\\0&0&A_{43}&A_{44}&A_{45}&A_{46}&0&0\\0&0&A_{53}&A_{54}&A_{55}&A_{56}&0&0\\0&0&0&0&A_{65}&A_{66}&A_{67}&A_{68}\\0&0&0&0&A_{75}&A_{76}&A_{77}&A_{88}\\0&0&0&0&0&0&A_{87}&A_{88}\end{bmatrix}$$

$$C=\begin{bmatrix}c_1^{\text{end}}\\c_2^{\text{end}}\\c_1^{\text{int}}\\c_2^{\text{int}}\\c_1^{\text{IEL}}\\c_2^{\text{IEL}}\\c_1^{\text{media}}\\c_2^{\text{media}}\end{bmatrix}\quad B=\begin{bmatrix}C^+_{\text{lumen}}\\0\\0\\0\\0\\0\\0\\0\end{bmatrix} \tag{36}$$

and the elements of the matrix A are given as follows:

$$A_{11}=1;\quad A_{12}=1$$
$$A_{21}=e^{\lambda_1^{end}L^*_{end}};\quad A_{22}=1;\quad A_{23}=-e^{\lambda_1^{int}L^*_{end}};\quad A_{24}=-1$$
$$A_{31}=v^*(1-\sigma_f^{end})e^{\lambda_1^{end}L^*_{end}}-\frac{1}{Pe^{end}}\lambda_1^{end}e^{\lambda_1^{end}L^*_{end}};$$
$$A_{32}=v^*(1-\sigma_f^{end});$$
$$A_{33}=-(v^*(1-\sigma_f^{int})e^{\lambda_1^{int}L^*_{end}}-\frac{1}{Pe^{int}}\lambda_1^{int}e^{\lambda_1^{int}L^*_{end}});$$
$$A_{34}=-v^*(1-\sigma_f^{int})$$
$$A_{43}=e^{\lambda_1^{int}(L^*_{end}+L^*_{int})};\quad A_{44}=1;$$
$$A_{45}=-e^{\lambda_1^{IEL}(L^*_{end}+L^*_{int})};\quad A_{46}=-1$$
$$A_{53}=v^*(1-\sigma_f^{int})e^{\lambda_1^{int}(L^*_{end}+L^*_{int})}-\frac{1}{Pe^{int}}\lambda_1^{int}e^{\lambda_1^{int}(L^*_{end}+L^*_{int})};$$
$$A_{54}=v^*(1-\sigma_f^{int});$$
$$A_{55}=-(v^*(1-\sigma_f^{IEL})(e^{\lambda_1^{IEL}(L^*_{end}+L^*_{int})}-\frac{1}{Pe^{IEL}}\lambda_1^{IEL}e^{\lambda_1^{IEL}(L^*_{endt}+L^*_{int})});$$
$$A_{56}=-v^*(1-\sigma_f^{IEL})$$
$$A_{65}=e^{\lambda_1^{IEL}(L^*_{end}+L^*_{int}+L^*_{IEL})};\quad A_{66}=1;$$
$$A_{67}=-e^{\lambda_1^{med}(L^*_{end}+L^*_{int}+L^*_{IEL})};\quad A_{68}=-e^{\lambda_2^{med}(L^*_{end}+L^*_{int}+L^*_{IEL})}$$
$$A_{75}=v^*(1-\sigma_f^{IEL})e^{\lambda_1^{IEL}(L^*_{end}+L^*_{int}+L^*_{IEL})}-\frac{1}{Pe^{IEL}}\lambda_1^{IEL}e^{\lambda_1^{IEL}(L^*_{endt}+L^*_{int}+L^*_{IEL})};$$
$$A_{76}=v^*(1-\sigma_f^{IEL});$$
$$A_{77}=-(v^*(1-\sigma_f^{med})e^{\lambda_1^{med}(L^*_{endt}+L^*_{int}+L^*_{IEL})}-\frac{1}{Pe^{med}}\lambda_1^{med}e^{\lambda_1^{med}(L^*_{end}+L^*_{int}+L^*_{IEL})});$$
$$A_{78}=-(v^*(1-\sigma_f^{med})e^{\lambda_2^{med}(L^*_{endt}+L^*_{int}+L^*_{IEL})}-\frac{1}{Pe^{med}}\lambda_2^{med}e^{\lambda_2^{med}(L^*_{end}+L^*_{int}+L^*_{IEL})})$$
$$A_{87}=\lambda_1^{med}e^{\lambda_1^{med}(L^*_{end}+L^*_{int}+L^*_{IEL}+L^*_{med})};$$
$$A_{88}=\lambda_2^{med}e^{\lambda_2^{med}(L^*_{end}+L^*_{int}+L^*_{IEL}+L^*_{med})} \tag{37}$$

Solution of the Eq. (35) can be presented as

$$C=A^{-1}B \tag{38}$$

Eqs. (23) and (38) are the compact form of the analytical solution for the LDL transport in the arterial wall.

4. Results and discussion

The analytical results for the LDL transport within the arterial wall can be achieved if proper physiological properties for each porous layer are provided. In the present study, all the parameter values are taken from Yang and Vafai [15]. The analytical results are compared with the numerical results presented in [15] for various physiological conditions. The computational geometry is shown in Fig. 1 [15]. In the numerical study, the mass transport of LDL through the lumen is coupled with the transport across the arterial wall, which is neglected in the analytical solution for simplicity.

4.1. Comparison between the analytical and numerical results at normal physiological conditions

The pressures at the lumen endothelium interface and media–adventitia interface for normal physiological conditions are chosen as 100 mmHg and 30 mmHg, respectively [15]. The resulting filtration velocity for the analytical solution is 2.28×10^{-5} mm/s. This is very close to the numerical filtration velocity of 2.31×10^{-5} mm/s at the mid-section longitudinally of the arterial geometry [15]. This suggests that the one-dimensional assumption for the filtration velocity is reasonable. The comparison of species profiles across the arterial wall between the analytical and numerical solutions is shown in Fig. 2, based on three different boundary conditions applied at the media–adventitia interface: $c/C_0=0$, $c/C_0=0.01$, and $\frac{\partial c}{\partial n}=0$. A slight difference is found between the analytical and numerical solutions within the intima and IEL. This is mainly due to the effect of transport in the axial direction, which is neglected in the analytical model. No pronounced difference is found between the boundary conditions of $c/C_0=0$ and $\frac{\partial c}{\partial n}=0$, from either the analytical or numerical solutions. This can be explained by the high absorption rate of LDL in the media, which makes the species distribution insensitive to different boundary conditions. One interesting aspect with respect to the species distribution is that a gradual concentration increase is found over the intima for both the analytical and numerical results. This is due to the barrier effect of IEL to large macromolecules such as LDL. All the numerical concentration results are taken at the longitudinal midsection of the computational geometry.

In general, the analytical solutions provide a good estimation of the LDL transport across the arterial wall, as long as only the straight circular geometry is considered.

4.2. Validation of the physiological parameters using the analytical solution

One of the major challenges for modeling of transport throughout an artery is the need for reliable experimental data for physiological parameters used in the model. For this purpose, a special effort is made for validating the physiological parameters. This is done through benchmarking against the experimental data of Meyer et al. [28]. The physiological parameters are taken directly from [15]. Yang and Vafai [15] have cited that the reaction coefficient k of 3.197×10^{-4} 1/s in the media is too high when compared to the experimental data of Meyer. Therefore two different reaction coefficients of 3.197×10^{-4} 1/s [7,15] and 1.4×10^{-4} 1/s [17,18] are examined in the present study for comparison. The results are displayed in Table 1. It is clear that the reaction coefficient of 1.4×10^{-4} 1/s provides a more reasonable species concentration

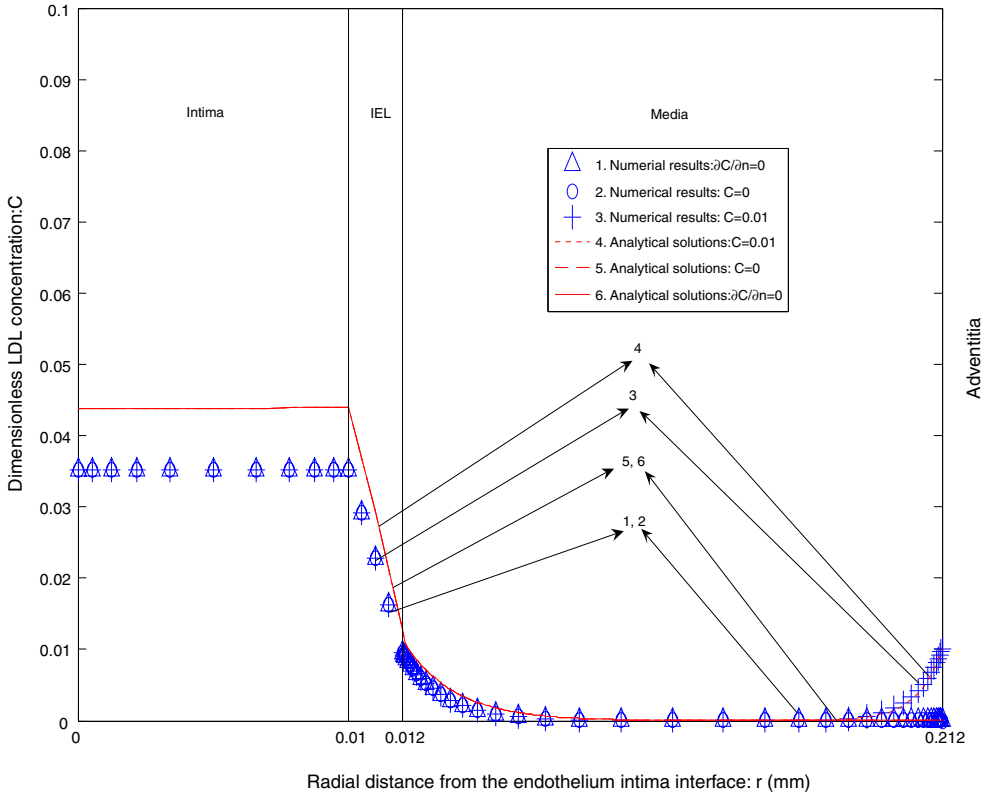

Fig. 2. Calculated species profiles across the intima, IEL and media layers.

Table 1
Summary of the values of the filtration velocity and species concentration taken from literature [16] and the present analytical model

		Meyer	Present model ($C=0$)	Present model ($C=0$)	Present model ($C=10^{-2}$)	Present model ($C=10^{-2}$)	Present model ($\partial C/\partial n=0$)	Present model ($\partial C/\partial n=0$)
Reaction coefficent (1/s)		N/A	3.197×10^{-4}	1.4×10^{-4}	3.197×10^{-4}	1.4×10^{-4}	3.197×10^{-4}	1.4×10^{-4}
Filtration velocity (mm/s)		1.78×10^{-5}	2.28×10^{-5}	2.28×10^{-5}	2.28×10^{-5}	2.28×10^{-5}	2.28×10^{-5}	2.28×10^{-5}
Species concentration	Lumen endothelium interface	1.026	1.0246	1.0246	1.0246	1.0246	1.0246	1.0246
	Intima IEL interface	N/A	4.436×10^{-2}	4.67×10^{-2}	4.436×10^{-2}	4.67×10^{-2}	4.436×10^{-2}	4.67×10^{-2}
	IEL media interface	1.00×10^{-2}	1.24×10^{-2}	1.63×10^{-2}	1.24×10^{-2}	1.63×10^{-2}	1.24×10^{-2}	1.63×10^{-2}
	Media ($r=3.214$ mm)	2.50×10^{-3}	3.443×10^{-5}	1.2×10^{-3}	3.459×10^{-5}	1.2×10^{-3}	3.443×10^{-5}	1.2×10^{-3}
	Media–adventitia interface	1.00×10^{-2}	0.00	0.00	1.00×10^{-2}	1.00×10^{-2}	1.152×10^{-7}	1.2675×10^{-4}

profile across the arterial wall when compared to 3.197×10^{-4} 1/s. As such, the reaction coefficient of 1.4×10^{-4} 1/s will be used in the present study.

4.3. Examining various pathological conditions

The effects of hypertension on the uptake of LDL by the arterial wall are studied using the new analytical model with the reaction coefficient of 1.4×10^{4} 1/s applied in the media. Four different cases, taken from [15], are studied. Case 1 is the baseline, which represents normal physiological condition. Cases 2 and 3 are used to test the effect of an increase in the transmural pressure, from 120 mmHg to 160 mmHg, respectively. The "stretching effect" of the pressure on the endothelium layer is studied in case 4. The pressure-linked "stretching effect" is due to an increase in the porosity of the endothelial layer associated with an increase in the pressure. For this reason, the endothelial LDL diffusivity is increased to 2.4×10^{-10} mm^2/s in case 4, consistent with what Stangeby and Ethier have cited in [5]. The three different species concentration boundary conditions are applied at the media–adventitia interface. One of the interesting effects of the hypertension on the LDL transport is the so called "concentration polarization",

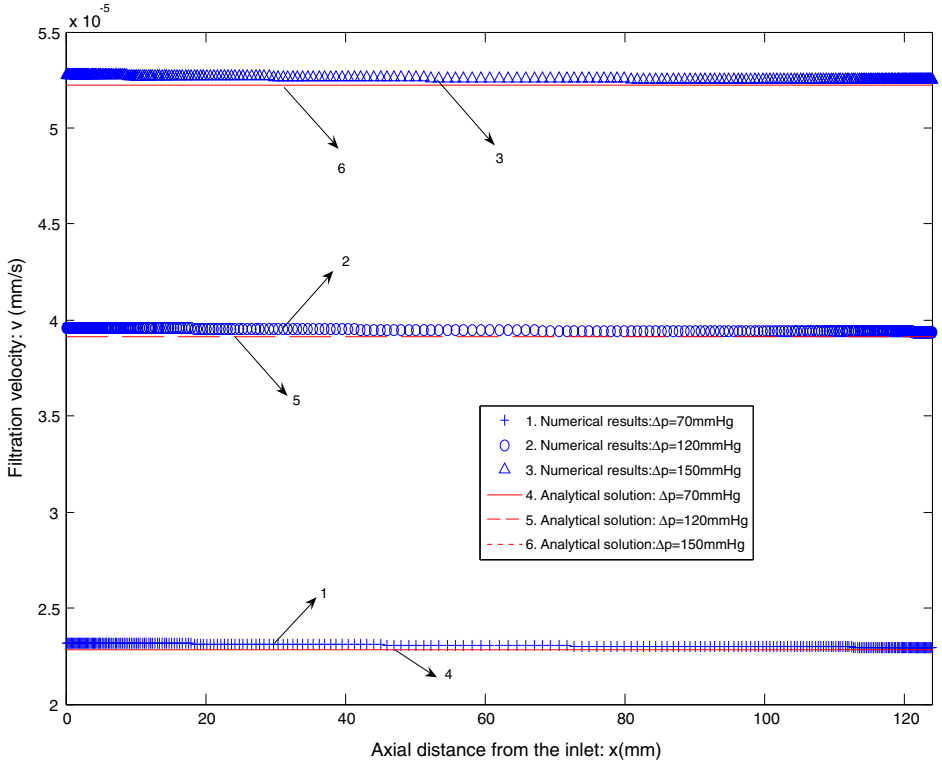

Fig. 3. Calculated filtration velocity profiles at the lumen endothelium interface along the axial direction.

which refers to the accumulation of LDL at the lumen endothelium interface. Yang and Vafai [15] have reported that concentration polarization plays a minor role in the transport of LDL in the arterial wall, especially in the IEL and media layers, mainly due to the barrier effect of the endothelium. As a result, the dimensionless concentration of LDL at the endothelium intima interface is chosen as 1.0246 for different conditions in the present study.

Fig. 3 demonstrates the effect of transmural pressure on the filtration velocity at the lumen endothelium interface.

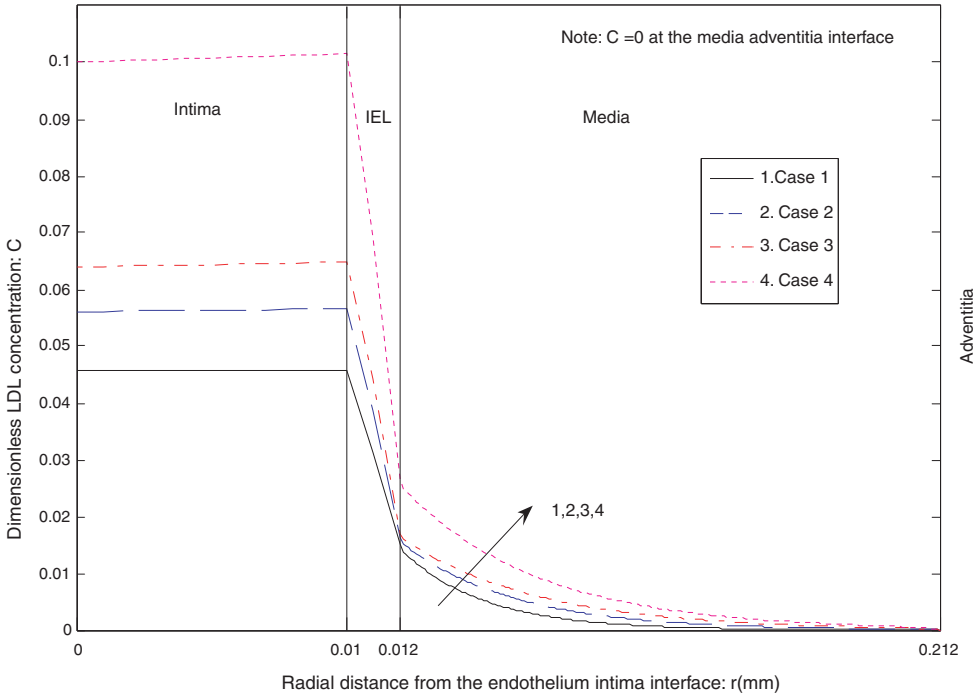

Fig. 4. Calculated species concentration across the intima, IEL and media.

As the transmural pressure increases, the magnitude of velocity increases correspondingly. Note that the analytical results are quite close to the numerical results for every case. Yang and Vafai have mentioned in [15] that the calculated velocity results for every case are well within the range of experimental measurements by Tedgui and Lever [19].

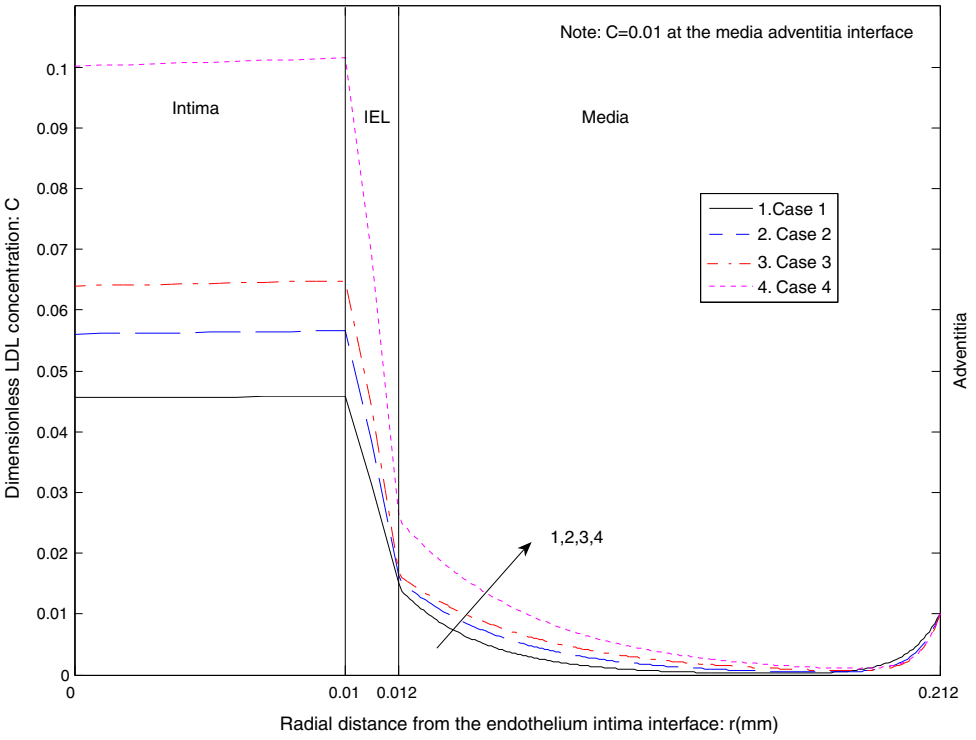

Fig. 5. Calculated species concentration across the intima, IEL and media.

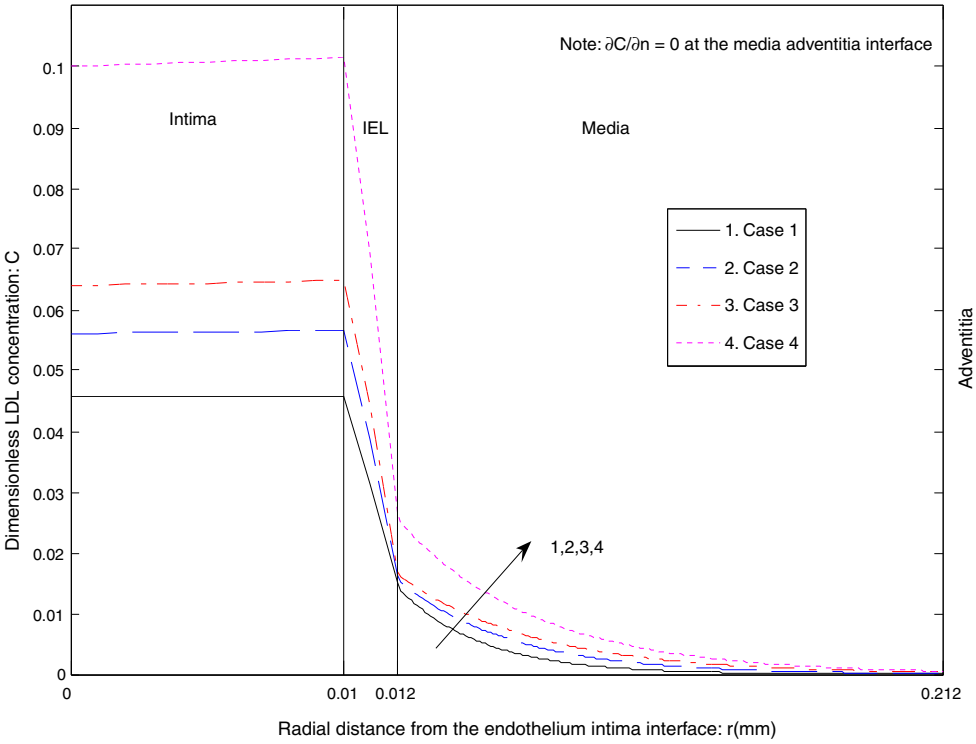

Fig. 6. Calculated species concentration across the intima, IEL and media.

The effects of hypertension on the species transport across the arterial wall are presented in Figs. 4–6, by demonstrating the species concentration profile across the intima, IEL and media based on the three different boundary conditions ($c/C_0 = 0$, $c/C_0 = 0.01$, and $\frac{\partial c}{\partial n} = 0$) at the media–adventitia interface respectively. All the results are calculated using the new analytical model. It is clear that the species concentration in the different layers increases dramatically from case 1 to case 4, which suggests that the pressure-driven flow and its associated endothelial diffusivity have a major effect on the transport of LDL across the arterial wall.

5. Conclusions

An analytical solution representing LDL transport through arteries is derived utilizing the primary transport in the lateral direction. The analytical solutions are found to be in good agreement with previously obtained comprehensive numerical results. The physiological parameters are validated using the derived analytical model. It is found that the reaction coefficient of 1.4×10^4 1/s gives a much more accurate species concentration across the wall when compared to other reaction coefficients available in the literature. Special attention is paid to the effects of hypertension. The analytical as well as the numerical results, indicate that the pressure-associated convective transport, combined with the pressure-induced increase in the endothelial porosity, result in more susceptibility to atherosclerosis for people with hypertension.

In general, it is evident that the four-layer porous model is a very powerful tool to model transport of LDL in the arterial wall and in investigating the formation of atherosclerosis. The derived analytical model is proven to be a reliable tool for estimating the LDL transport in a straight circular geometry. One interesting aspect of future work is to examine the effects of curvature on the transport of the LDL transport in the arterial wall.

References

[1] G. Rappitsch, K. Perktold, Pulsatile albumin transport in large arteries: a numerical simulation study, J. Biomech. Eng. 118 (1996) 511–519.

[2] G. Rappitsch, K. Perktold, E. Pernkopf, Numerical modeling of shear-dependent mass transfer in large arteries, Int. J. Numer. Methods Fluids 25 (1997) 847–857.

[3] S. Wada, T. Karino, Computational study on LDL transfer from flowing blood to arterial walls, in: T. Yamaguchi (Ed.), Clinical Applications of Computational Mechanics to the Cardiovascular System, Springer, Berlin, 2000, pp. 157–173.

[4] S. Wada, T. Karino, Theoretical prediction of low-density lipoproteins concentration at the luminal surface of an artery with a multiple bend, Ann. Biomed. Eng. 30 (2002) 778–791.

[5] D.K. Stangeby, C.R. Ethier, Coupled computational analysis of arterial LDL transport – effects of hypertension, Comp. Methods Biomech. Biomed. Eng. 5 (2002) 233–241.

[6] D.K. Stangeby, C.R. Ethier, Computational analysis of coupled blood-wall arterial LDL transport, J. Biomech. Eng. 124 (2002) 1–8.

[7] M. Prosi, P. Zunino, K. Perktold, A. Quarteroni, Mathematical and numerical models for transfer of low-density lipoproteins through the arterial walls: a new methodology for the model set up with applications to the study of disturbed luminal flow, J. Biomech. 38 (2005) 903–917.

[8] F. Yuan, S. Chien, S. Weinbaum, A new view of convective–diffusive transport processes in the arterial intima, J. Biomech. Eng. 133 (1991) 314–329.

[9] Y. Huang, D. Rumschitzki, S. Chien, S. Weinbaum, A fiber matrix model for the growth of macromolecular leakage spots in the arterial intima, J. Biomech. Eng. 116 (1994) 430–445.

[10] Z.J. Huang, J.M. Tarbell, Numerical simulation of mass transfer in porous media of blood vessel walls, Am. J. Physiol. 273 (1997) H464–H477.

[11] S. Tada, J.M. Tarbell, Internal elastic lamina affects the distribution of macromolecules in the arterial wall: a computational study, Am. J. Physiol. 287 (2004) H905–H913.

[12] D.L. Fry, Mathematical models of arterial transmural transport, Am. J. Physiol. 248 (1985) H240–H263.

[13] D.L. Fry, Mass transport, atherogenesis and risk, Arteriosclerosis 7 (1987) 88–100.

[14] G. Karner, K. Perktold, H.P. Zehentner, Computational modeling of macromolecule transport in the arterial wall, Comput. Methods Biomech. Biomed. Eng. 4 (2001) 491–504.

[15] N. Yang, K. Vafai, Modeling of low-density lipoprotein (LDL) transport in the artery – effects of hypertension, J. Int. Heat Mass Transfer 49 (2006) 850–867.

[16] G. Meyer, R. Merval, A. Tedgui, Effects of pressure-induced stretch and convection on low-density lipoprotein and albumin uptake in the rabbit aortic wall, Circ. Res. 79 (1996) 532–540.

[17] G.A. Truskey, Low density lipoprotein transport and metabolism in the arterial wall, Ph.D. thesis, Massachusetts Institute of Technology, Cambridge, MA, 1985.

[18] E.D. Morris, G.M. Saidel, G.M. Chisolm, Optimal design of experiments to estimate LDL transport parameters in arterial wall, Am. J. Physiol. 261 (1991) H929–H949.

[19] A. Tedgui, M.J. Lever, Filtration through damaged and undamaged rabbit thoracic aorta, Am. J. Physiol. 247 (1984) H784–H791.